

Exciton insulators in two-dimensional systems

Huaiyuan Yang(杨怀远), Xi Dai(戴希), and Xin-Zheng Li(李新征)
Citatio: Chin. Phys. B, 2025, 34 (**9**): 097301. DOI: 10.1088/1674-1056/ade3ae
http://cpb.iphy.ac.cn; http://iopscience.iop.org/cpb

What follows is a list of articles you may be interested in

Moiré physics in two-dimensional materials: Novel quantum phases and electronic properties

Zi-Yi Tian(田子弈), Si-Yu Li(李思宇), Hai-Tao Zhou(周海涛), Yu-Hang Jiang(姜宇航), and Jin-Hai Mao(毛金海)
Chin. Phys. B, 2025, 34 (**2**): 027301. DOI: 10.1088/1674-1056/ad9e96

$GaInX_3$ (X = S, Se, Te): Ultra-low thermal conductivity and excellent thermoelectric performance

Zhi-Fu Duan(段志福), Chang-Hao Ding(丁长浩), Zhong-Ke Ding(丁中科), Wei-Hua Xiao(肖威华), Fang Xie(谢芳), Nan-Nan Luo(罗南南), Jiang Zeng(曾犟), Li-Ming Tang(唐黎明), and Ke-Qiu Chen(陈克求)
Chin. Phys. B, 2024, 33 (**8**): 087302. DOI: 10.1088/1674-1056/ad47e3

Effect of strain on structure and electronic properties of monolayer C_4N_4

Hao Chen(陈昊), Ying Xu(徐瑛), Jia-Shi Zhao(赵家石), and Dan Zhou(周丹)
Chin. Phys. B, 2024, 33 (**5**): 057302. DOI: 10.1088/1674-1056/ad260c

Anomalous valley Hall effect in two-dimensional valleytronic materials

Hongxin Chen(陈洪欣), Xiaobo Yuan(原晓波), and Junfeng Ren(任俊峰)
Chin. Phys. B, 2024, 33 (**4**): 047304. DOI: 10.1088/1674-1056/ad1c59

Improving the electrical performances of InSe transistors by interface engineering

Tianjun Cao(曹天俊), Song Hao(郝松), Chenchen Wu(吴晨晨), Chen Pan(潘晨), Yudi Dai(戴玉頔), Bin Cheng(程斌), Shi-Jun Liang(梁世军), and Feng Miao(缪峰)
Chin. Phys. B, 2024, 33 (**4**): 047302. DOI: 10.1088/1674-1056/ad24d7

TOPICAL REVIEW — Exciton physics: Fundamentals, materials and devices

Exciton insulators in two-dimensional systems

Huaiyuan Yang(杨怀远)[1], Xi Dai(戴希)[1,†], and Xin-Zheng Li(李新征)[2,3,4,‡]

[1] *Department of Physics, Hong Kong University of Science and Technology, Kowloon* 999077, *Hong Kong, China*

[2] *State Key Laboratory for Artificial Microstructure and Mesoscopic Physics, Frontier Science Center for Nano-optoelectronics and School of Physics, Peking University, Beijing* 100871, *China*

[3] *Interdisciplinary Institute of Light-Element Quantum Materials, Research Center for Light-Element Advanced Materials, and Collaborative Innovation Center of Quantum Matter, Peking University, Beijing* 100871, *China*

[4] *Peking University Yangtze Delta Institute of Optoelectronics, Nantong* 226010, *China*

(Received 1 May 2025; revised manuscript received 9 June 2025; accepted manuscript online 12 June 2025)

Electron–hole interactions play a crucial role in determining the optoelectronic properties of materials, and in low-dimensional systems this is especially true due to the decrease of screening. In this review, we focus on one unique quantum phase induced by the electron–hole interaction in two-dimensional systems, known as "exciton insulators" (EIs). Although this phase of matter has been studied for more than half a century, suitable platforms for its stable realization remain scarce. We provide an overview of the strategies to realize EIs in accessible materials and structures, along with a discussion on some unique properties of EIs stemming from the band structures of these materials. Additionally, signatures in experiments to distinguish EIs are discussed.

Keywords: excitonic insulator, two-dimensional materials

PACS: 73.20.Mf, 73.22.Gk, 71.35.–y

DOI: 10.1088/1674-1056/ade3ae **CSTR:** 32038.14.CPB.ade3ae

1. Introduction

Exciting an electron from the valence band of the ground state of a semiconductor to the conduction band creates an electron–hole pair. Due to the opposite charges carried by the electron and hole, there is an attractive Coulomb interaction between them, leading to the formation of a stable two-body bound state. This quasi-particle is called an "exciton", first proposed by Frenkel and Wannier in the early 1930s.[1,2] The intrinsic connection between exciton and optical excitation means that excitons determine the optoelectronic properties of these semiconductors to a large extent.[3] In two-dimensional (2D) and quasi-2D materials, the screening effects of the electrons are weaker, and the Coulomb interactions are stronger. This may lead to large exciton binding energies. In the meantime, bright excitons also exhibit strong oscillator strengths.[4,5] As such, the optical properties of 2D materials can be more substantially altered by excitons compared with their bulk correspondences. In recent years, many 2D materials with interesting optical properties have been reported, including transition-metal dichalcogenides, halide perovskites, and layered heterostructures,[6–8] as demonstrated by their optical absorption or photoluminescence spectra.

Underlying the theoretical descriptions of the exciton properties is the single-particle excitation spectra of the electronic system. In periodic systems, this is called the electronic band structure, and the corresponding theory is called band theory.[9] For condensed matter physics, it is the most successful theoretical framework used for the description of excitations. On top of it, if one combines its most fundamental quantity, i.e., the band gap, with the most fundamental quantity of excitons, i.e., the exciton binding energy, a very interesting scenario may arise, as proposed by Keldysh, Kohn, Rice, and others in the 1960s.[10–13] If the exciton binding energy exceeds the band gap, the formation of excitons becomes energetically favorable, rather than ordinary band structures. Under appropriate conditions, excitons can spontaneously form in large quantities and undergo condensation as bosonic particles, exhibiting exotic transport and optical properties, and becoming insulating for electron transport.[10–18] As such, this new quantum phase is called an exciton insulator (EI) phase, routinely obtained from the normal band phase in some special materials upon decreasing temperatures.[19–21]

Despite the simplicity of this physical picture and the long history of this idea, theoretical and experimental studies of this phenomenon were both quite limited for a long time. There are two main restrictions. The first one is on the stringent requirements for the existence of this quantum phase, as reflected by the fact that large exciton binding energies are required. Intrinsic materials possessing feasible band structures for this are rare. For example, in bulk materials, the large screening

†Corresponding author. E-mail: daix@ust.hk

‡Corresponding author. E-mail: xzli@pku.edu.cn

© 2025 Chinese Physical Society and IOP Publishing Ltd. All rights, including for text and data mining, AI training, and similar technologies, are reserved.

due to the many-body nature of the electrons means that there are not many materials with a large exciton binding energy. The second one is that even though this new phase exists, it is difficult to characterize in experiments.[22,23] Taking the most often used technique, i.e., electron transport measurement, as an example, the neutrality of the electron–hole pair means that zero net charge can be measured by the transport of the excitons, unless the electron and hole go through different channels. As such, solid identifications of this EI phase in realistic materials remain scarce.[18,24]

In recent years, studies on 2D materials and heterostructures mean that amelioration of both conditions discussed above appears.[25–28] The decrease of screening in 2D materials means that the exciton binding energies can be large and a new scenario when it exceeds the band gap may exist. In the meantime, advances in experimental techniques, e.g., angle-resolved photoemission spectroscopy (ARPES), scanning tunneling microscopy (STM), and delicate high-precision electric transport experiments, also mean that fingerprinting this new quantum phase becomes possible.[29–34] Based on this progress, we write this review to discuss some new progress in the research on EIs from a theoretical perspective, together with some discussions of the novel properties of EIs. Results reported in three of our previously published papers, Refs. [19–21], are selected as the basis for these discussions. Our focus is to provide an overview of the strategies used to realize realistic EI systems. With a summary of previous results and an illustration of the strategies we take to search for EIs, we hope that the methods used in this review can help to guide the discovery of EIs in more realistic systems and their characterization in experiments.

The paper is organized as follows. In Section 2, we give a brief introduction to the theory used to describe EIs using a Bardeen–Cooper–Schrieffer (BCS)-like equation. In Section 3, we discuss the strategies used to realize intrinsic EIs in 2D materials and give several examples using results of state-of-the-art first-principles calculations. In Section 4, we discuss EIs in heterostructures and demonstrate a way to find high-angular momentum EIs. In Section 5, we summarize the whole review and give a perspective on the open questions.

2. General description

In this section, we use the mean-field BCS-like theory to describe the EI state.[11,12] Consider the simplest case with one conduction band and one valence band, the interaction between the electrons and holes can be written as

$$\begin{aligned} H \;=\; & \sum_{\boldsymbol{k}} \varepsilon_c(\boldsymbol{k}) a^{\dagger}_{c\boldsymbol{k}} a_{c\boldsymbol{k}} + \sum_{\boldsymbol{k}} \varepsilon_v(\boldsymbol{k}) a^{\dagger}_{v\boldsymbol{k}} a_{v\boldsymbol{k}} \\ & + \sum_{\boldsymbol{k},\boldsymbol{k}',\boldsymbol{q}} V(\boldsymbol{q}) a^{\dagger}_{v\boldsymbol{k}+\boldsymbol{q}} a_{v\boldsymbol{k}} a^{\dagger}_{c\boldsymbol{k}'-\boldsymbol{q}} a_{c\boldsymbol{k}'}. \end{aligned} \tag{1}$$

Here $V(\boldsymbol{q})$ is the attractive Coulomb interaction, $a^{\dagger}_{c\boldsymbol{k}}$ ($a_{c\boldsymbol{k}}$) and $a^{\dagger}_{v\boldsymbol{k}}$ ($a_{v\boldsymbol{k}}$) are the creation (annihilation) operators of the conduction and valence bands, and $\varepsilon_c(\boldsymbol{k})$ and $\varepsilon_v(\boldsymbol{k})$ are the energy dispersions near the conduction and valence band edges, respectively. Expressions of $\varepsilon_c(\boldsymbol{k})$ and $\varepsilon_v(\boldsymbol{k})$ follow the effective mass model

$$\varepsilon_c(\boldsymbol{k}) = \frac{G}{2} + \frac{\boldsymbol{k}^2}{2m}, \quad \varepsilon_v(\boldsymbol{k}) = -\frac{G}{2} - \frac{\boldsymbol{k}^2}{2m}, \tag{2}$$

where m is the mass. The G is the band gap, with $G > 0$ ($G < 0$) representing semiconductors (semimetals).

Then, we can define the EI order parameter to be

$$\Delta(\boldsymbol{k}) \equiv -\sum_{\boldsymbol{k}'} V\left(\boldsymbol{k}-\boldsymbol{k}'\right) \left\langle a^{\dagger}_{c\boldsymbol{k}'} a_{v\boldsymbol{k}'} \right\rangle. \tag{3}$$

Substituting it into Eq. (1), we have

$$\begin{aligned} H \;=\; & \sum_{\boldsymbol{k}} \varepsilon_c(\boldsymbol{k}) a^{\dagger}_{c\boldsymbol{k}} a_{c\boldsymbol{k}} + \sum_{\boldsymbol{k}} \varepsilon_v(\boldsymbol{k}) a^{\dagger}_{v\boldsymbol{k}} a_{v\boldsymbol{k}} \\ & + \sum_{\boldsymbol{k}} \left(\Delta(\boldsymbol{k}) a^{\dagger}_{c\boldsymbol{k}} a_{v\boldsymbol{k}} + \text{h.c.} \right) \\ & + \sum_{\boldsymbol{k}} \Delta(\boldsymbol{k}) \left\langle a^{\dagger}_{c\boldsymbol{k}} a_{v\boldsymbol{k}} \right\rangle. \end{aligned} \tag{4}$$

After diagonalization, the energy eigenvalues are

$$E_{\alpha}(\boldsymbol{k}) = \xi_{\boldsymbol{k}} - E_{\boldsymbol{k}}, \quad E_{\beta}(\boldsymbol{k}) = \xi_{\boldsymbol{k}} + E_{\boldsymbol{k}}. \tag{5}$$

Here $\xi_{\boldsymbol{k}} = (\varepsilon_c(\boldsymbol{k}) - \varepsilon_v(\boldsymbol{k}))/2$ and $E_{\boldsymbol{k}} = \sqrt{\xi^2_{\boldsymbol{k}} + |\Delta(\boldsymbol{k})|^2}$. The gap equation is

$$\Delta(\boldsymbol{k}) = \sum_{\boldsymbol{k}'} V(\boldsymbol{k}-\boldsymbol{k}') \frac{\Delta(\boldsymbol{k}')}{2E_{\boldsymbol{k}'}} \tanh \frac{E_{\boldsymbol{k}'}}{2k_{\mathrm{B}}T}, \tag{6}$$

which is nearly identical to the BCS gap equation for superconductivity.[12]

After solving Eq. (6) self-consistently, a nonzero $\Delta(\boldsymbol{k})$ means that the EI state is the ground state. The wavefunction of this EI state can be written as[12]

$$|\Psi_{\mathrm{EI}}\rangle = \prod_{\boldsymbol{k}} \left(u^{*}_{\boldsymbol{k}} - v^{*}_{\boldsymbol{k}} a^{\dagger}_{c\boldsymbol{k}} a_{v\boldsymbol{k}} \right) |\Psi_{\mathrm{N}}\rangle. \tag{7}$$

Here $|\Psi_{\mathrm{N}}\rangle$ is the noncondensing normal state described by the band theory, with a fully occupied valence conduction band and an empty occupied band, and $u_{\boldsymbol{k}}$s and $v_{\boldsymbol{k}}$s are the normalized coefficients that diagonalize Eq. (4). The wavefunction in Eq. (7) means that the form of the EI state is very similar to the BCS superconducting state,[35] with excitons playing the role of Cooper pairs.

From the perspective of symmetry breaking, the superconducting phase transition breaks charge conservation, corresponding to the breaking of $U(1)$ symmetry; while exciton condensation reduces the conservation of electron and hole numbers to the conservation of their sum, which corresponds to the symmetry reduction from $U(1) \times U(1)$ to $U(1)$. Unlike the Cooper pairs in superconductors, the formation of excitons does not require mediators like phonons or other bosons, since

there is an intrinsic attractive interaction between electrons and holes. In addition, excitons are electrically neutral, meaning that EIs do not exhibit supercurrent transport properties as in superconductors. Other forms of superfluidity, however, may exist.[36]

The normal state before condensation can be a semiconductor or semimetal. In the case of a semiconductor (i.e., the band gap is positive), Coulomb interactions are weakly screened due to the absence of free charge carriers in the system, resulting in a strong attraction between electrons and holes. As a result, the excitons have a large binding energy with small radius and low density, and excitons already exist before condensation occurs. As the temperature decreases, condensation occurs when the de Broglie wavelength of the excitons becomes comparable to the average distance between them. Therefore, these EIs can be considered as a Bose–Einstein condensate (BEC) of excitons.

When the normal state is a semimetal, the presence of free charge carriers strongly screens the Coulomb interaction. Therefore, the attraction between electrons and holes is normally weak. This leads to smaller binding energy, larger radius, and higher density of excitons, with no excitons preformed before condensation. Thus, these EIs are similar to the BCS state in normal superconductors.[35] Both BCS-type and BEC-type EIs exist in realistic systems, and a transition between these two types can be realized by adjusting physical parameters such as the band gap, interaction strength, or exciton density. The characteristic of this transition is not like a phase transition, but rather a crossover, known as the BCS–BEC crossover.[37–41]

3. Intrinsic materials

Over the past half-century, significant efforts have been devoted to the search for EIs, leading to substantial theoretical and experimental progress. Two well-known examples are 1T-$TiSe_2$[42,43] and Ta_2NiSe_5.[44–46] However, both materials exhibit phonon-induced lattice instabilities at low temperatures, complicating the determination of whether the phase transition is driven by excitonic mechanisms. Other artificial systems, such as InAs/GaSb quantum wells[22] and $MoSe_2$/WSe_2 bilayers,[29] require precise atomic-level control, which may impede the broader application of EIs. As such, there is a need to explore more intrinsic EI materials with stable lattices.

3.1. General strategies

To realize an EI, a large exciton binding energy (E_b) is essential. This requires weak screening effects, which can be achieved in low-dimensional systems. However, Choi *et al.* found that in typical two-dimensional systems, the exciton binding energy E_b linearly depends on the band gap E_g.[47] This implies that as E_b increases, E_g also increases, with E_b always remaining smaller than E_g. This proportional relationship can be qualitatively understood in terms of the screening effect.[48] As the screening weakens in semiconductors, the band gap increases, and similarly, the exciton binding energy increases, resulting in a positive correlation between E_b and E_g.

To break this synergy, there are two strategies. The first one is to focus on excitons formed by band edges that do not involve dipole transitions.[25–27] The second one is to enhance the overlap between electron and hole wavefunctions, making the interaction between them less sensitive to the screening effects from surrounding electrons.[28] These strategies have been employed in several prior works, predicting many intrinsic EIs, such as two-dimensional GaAs,[25] 1T-$NiCl_2$,[26] graphone,[27] and a bilayer kagome material.[28]

We are adopting both strategies in the search for new 2D EIs. For a better understanding of our results, we start with a brief introduction to the physics behind the synergy, as provided in Ref. [48]. In 2D systems, the static dielectric function can be described as

$$\varepsilon(\boldsymbol{q}) = 1 + 2\pi\alpha_{2D}|\boldsymbol{q}|, \tag{8}$$

where α_{2D} is the two-dimensional polarizability, characterizing the strength of screening. Its specific form is

$$\alpha_{2D} = \frac{2e^2}{(2\pi)^2}\sum_{c,v}\int_{\boldsymbol{k}}\frac{|\langle u_{c,\boldsymbol{k}}|\nabla_{\boldsymbol{k}}|u_{v,\boldsymbol{k}}\rangle|^2}{E_{c,\boldsymbol{k}} - E_{v,\boldsymbol{k}}}\mathrm{d}^2\boldsymbol{k}. \tag{9}$$

From this equation, it is clear that when the band gap is small, α_{2D} becomes large, resulting in a strong screening effect, which in turn reduces the exciton binding energy. However, if at the band edges $|\langle u_{c,\boldsymbol{k}}|\nabla_{\boldsymbol{k}}|u_{v,\boldsymbol{k}}\rangle| = 0$, even if $E_{c,\boldsymbol{k}} - E_{v,\boldsymbol{k}}$ is very small, its effect on α_{2D} is negligible. As such, excitons formed at the band edges could have a binding energy larger than the band gap itself, thus forming an EI.

In addition, Eq. (9) also suggests that α_{2D} is only associated with direct transitions, i.e., transitions between states with the same $\boldsymbol{k}$. For indirect band gap semiconductors, the binding energy of the indirect exciton, which is characterized by physical quantities such as α_{2D} that describe screening, is primarily related to the direct band gap rather than the indirect band gap. Thus, if the indirect band gap is small while the direct gap is large, the screening is also weak, and the exciton binding energy can be large. In this case, the exciton binding energy can exceed the indirect band gap, and it becomes possible to realize an EI with an indirect band gap. Additionally, we found that in two-dimensional materials with a small indirect band gap, the EI may also exhibit a higher transition temperature T_C.[19] This can be qualitatively demonstrated through a simple analysis of the gap equation shown in Eq. (6), which indicates that strong Coulomb interactions $V(\boldsymbol{q})$ and a small band gap can lead to a large order parameter. Consequently, the transition temperature T_C increases.

Based on this analysis, in Subsections 3.2 and 3.3, we focus on systems which satisfy the following two conditions: (i) 2D materials with an indirect band gap, and (ii) 2D semiconductors with the same parities at the band edges, in order to achieve a more pronounced EI phase transition.

3.2. The 2D materials with an indirect band gap

In Ref. [19], we used the above condition (i) to search for EIs. Specifically, we conducted an extensive search within transition-metal dichalcogenides (TMDs) building on previous computational works,[49,50] and identified two potential EIs: $2H$-$TiTe_2$ and $1T$-$PdTe_2$, whose lattice structures are shown in Figs. 1(a) and 1(b). The black lines in Figs. 1(c) and 1(d) show their Perdew–Burke–Ernzerhof (PBE) band structures. The former is an indirect band gap semiconductor, while the latter is a semimetal. The band gap of $2H$-$TiTe_2$ is 53 meV, while the band overlap in $1T$-PdTe2 is 107 meV. Since PBE calculations typically underestimate the band gap E_g, this work performed G_0W_0 calculations based on the PBE band structures. The results are shown as the red lines in Figs. 1(c) and 1(d). After the G_0W_0 corrections, both $2H$-$TiTe_2$ and $1T$-$PdTe_2$ become indirect semiconductors, with band gaps of 276 meV and 387 meV, respectively. For $2H$-$TiTe_2$, the valence band maximum (VBM) and conduction band minimum (CBM) are located at the Γ and M points, respectively. For $1T$-$PdTe_2$, they are located at the Γ and $N^{'}$ points (the midpoint of ΓM).

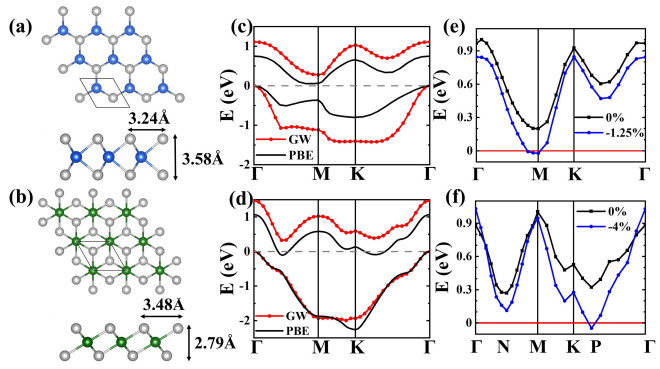


Fig. 1. Side (top) and top (bottom) views of the pristine structures of (a) $2H$-$TiTe_2$ and (b) $1T$-$PdTe_2$. Blue, grey, and green balls denote the Te, Ti, and Pd atoms, respectively. (c), (d) The PBE (black solid lines) and G_0W_0 (red lines of solid circles) band structures for the primitive $2H$-$TiTe_2$ and $1T$-$PdTe_2$. The grey dashed lines indicate the energy of the VBM. (e), (f) Dispersions of the lowest energy exciton states for (e) $2H$-$TiTe_2$ and (f) $1T$-$PdTe_2$. The red lines indicate zero excitation energy. This figure is adopted from Ref. [19].

On top of these band structures, we performed finite-momentum Bethe–Salpeter equation (BSE) calculations to obtain the lowest-energy excitonic states. The exciton wavefunction at finite momentum $\boldsymbol{Q}$ reads

$$\chi^{\boldsymbol{Q}}(\boldsymbol{r}_e, \boldsymbol{r}_h) = \sum_{vc\boldsymbol{k}} A_{v\boldsymbol{k},c\boldsymbol{k}+\boldsymbol{Q}}\, \psi^*_{c\boldsymbol{k}+\boldsymbol{Q}}(\boldsymbol{r}_e)\, \psi_{v\boldsymbol{k}}(\boldsymbol{r}_h). \quad (10)$$

Here $A_{v\boldsymbol{k},c\boldsymbol{k}+\boldsymbol{Q}}$ is the exciton envelope function, $\psi_{c\boldsymbol{k}}$ ($\psi_{v\boldsymbol{k}}$) is the electron (hole) Bloch wavefunction. The exciton dispersions of the lowest excitons in both materials are shown as the black lines in Figs. 1(e) and 1(f). One surprising result is that the lowest-energy exciton in $1T$-$PdTe_2$ is located at the P point ($KP = \Gamma K/4$), rather than at the N point, where the CBM resides. The EI phase transition requires the exciton energy to be negative. However, neither of these materials meets this condition, and as such, no exciton phase transition occurs.

Then, we apply strain to them, since strain can significantly reduce the band gap in such two-dimensional materials.[51] This is enabled by adjusting the lattice constants of the materials in the first-principles calculations.[25,49] Our results show that the band gap in $2H$-$TiTe_2$ decreases rapidly with increasing strain, reaching 28 meV at -1.25% strain, while the corresponding exciton binding energy decreases slightly to 49 meV. This indicates that an EI phase transition occurs at -1.25% strain, as shown in Fig. 1(e), where a negative-energy exciton state appears near the M point. For $1T$-$PdTe_2$, the CBM shifts to the P point at -4% strain, as shown in Fig. 1(f), and the exciton binding energy E_b and the indirect band gap are 63 meV and 16 meV, respectively. Therefore, an EI phase emerges in $1T$-$PdTe_2$ under approximately -4% strain.

In other potential EIs, such as $1T$-$TiSe_2$[42,43] and Ta_2NiSe_5,[44–46] the EI phase transition is accompanied by phonon softening. This makes it challenging to distinguish the dominant mechanism of the phase transition — whether excitonic effects or phonon effects prevail. In Fig. 2 of Ref. [19], we show that in the phonon spectra for $2H$-$TiTe_2$ and $1T$-$PdTe_2$ there are no soft phonons. Therefore, both are stable in the absence of electron–hole interactions. If experimental observations reveal lattice instability or charge density wave (CDW) phenomena, it would undoubtedly be caused by the excitonic effects. In experiments, such EI phase transitions can be detected by angle-resolved photoemission spectroscopy (ARPES), where a band gap for the quasiparticle excitations emerges. Furthermore, STM and other methods can potentially reveal charge density waves associated with finite-momentum exciton phase transitions. We expect some experimental observations along this direction.

Despite the purity of the theoretical origin due to EI for the possible experimental signatures as discussed above, we note that both of these materials are difficult to grow experimentally. $2H$-$TiTe_2$ has only been grown on Au surfaces. We hope that experimental researchers can overcome these challenges, and that the methods proposed in this chapter can guide the discovery of more intrinsic EIs like these. In fact, recent experiments have already confirmed the existence of EIs in the indirect band gap two-dimensional semiconductor WTe_2 and the indirect two-dimensional semimetal $HfTe_2$.[32,33,52] The atomic and band structures of $HfTe_2$ are highly similar to those of $PdTe_2$. This provides indirect support for the predictions made here and in Ref. [19].

3.3. Band edges with same parity in QSHIs

Besides the factor of indirect band gap, the second strategy is to break the synergy between E_g and E_b in 2D materials and to play with the parity of the CBM and VBM states, mentioned above as condition (ii) at the end of Subsection 3.1. Along this route, we will show one example when EIs can exist in quantum spin-Hall insulators (QSHIs). Conventional research on QSHIs focuses on the fact that their bulk bands have a gap, making them insulating. The edge states, on the other hand, are gapless. This allows for dissipationless helical transport at the system's boundary,[53–58] closely related to the nontrivial topological nature of their energy bands. In Ref. [21], we searched for EIs with such topological properties in QSHIs.

Specifically, we search for QSHIs with spatial inversion symmetry, where the band inversion occurs not between the CBM and VBM, but rather between distant bands and the combination of CBM and VBM. If the band inversion happens between the CBM and VBM, the Fu–Kane criterion[59] dictates that, in order for the system's Z_2 topological index to be nontrivial, the CBM and VBM must have opposite parities. On the other hand, if the band inversion occurs between distant bands and the combination of CBM and VBM, the CBM and VBM can have the same parity. In this case, the energy gap between the CBM and VBM can be opened by spin–orbit coupling (SOC). As a result, dipole transitions between the band edges are restricted due to their matching parity, making it possible to realize an EI. Similar conclusions were previously reported in Ref. [60].

In Ref. [21], we showed that 2D QSHIs AsO and $Mo_2TiC_2O_2$ are potential EIs.[61,62] Their lattice structures are shown in Figs. 2(a) and 2(c), where it can be seen that AsO has a structure similar to hexagonal 2D-decorated stanene,[62,62] and $Mo_2TiC_2O_2$ is a typical material of the MXene family.[61] They both have C_3 rotational symmetry and inversion symmetry, and the band inversion happens at the Γ point between the p_z orbital with negative parity and the $p_x \pm ip_y$ ones with positive parity in AsO, and between the d_{z^2} orbital with negative parity and the $d_{xy} \pm i d_{x^2-y^2}$ ones with positive parity in $Mo_2TiC_2O_2$. Among these orbitals, the p_z and d_{z^2} orbitals are far from the Fermi level, while the $p_x \pm ip_y$ and $d_{xy} \pm i d_{x^2-y^2}$ orbitals lie close to the Fermi surface (Figs. 2(b) and 2(d)), and the SOC opens a band gap in these orbitals.[61,62,64] The G_0W_0 band gaps of AsO and $Mo_2TiC_2O_2$ are 165 meV and 115 meV, respectively. BSE calculations further show that the lowest energy exciton binding energies obtained for these materials are ~ 300 meV and ~ 350 meV, respectively. This is mainly due to the fact that the edge states of AsO and $Mo_2TiC_2O_2$ have the same parity. Thus, the exciton binding energies exceed the band gaps, indicating that an EI phase transition can be expected to occur in both materials.

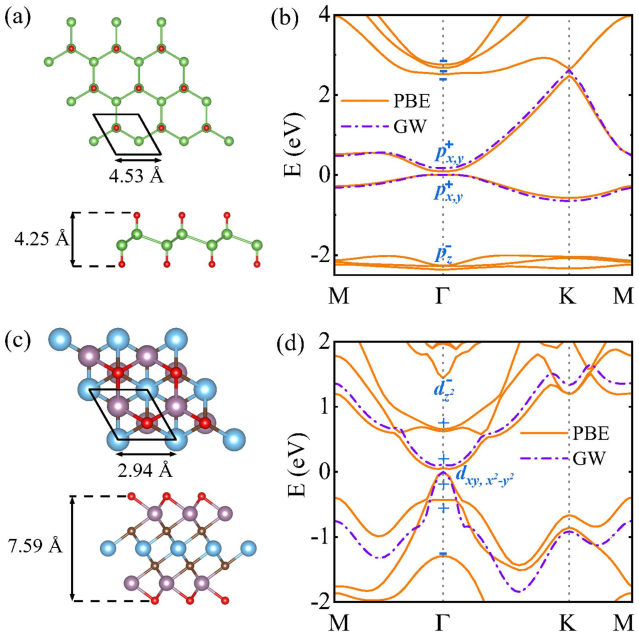


Fig. 2. (a), (c) Top (top) and side (bottom) views of the atomic structures of (a) AsO and (c) $Mo_2TiC_2O_2$. Green, red, blue, purple, and brown balls denote the As, O, Ti, Mo, and C atoms, respectively. (b), (d) The PBE (orange solid lines) and *GW* (purple dot-dashes lines) band structures of (b) AsO and (d) $Mo_2TiC_2O_2$. The blue symbols mark the parity of the bands near the Fermi level. This figure is adopted from Ref. [21].

On the basis of $\{|p_x + ip_y,\uparrow\rangle,\ |p_x + ip_y,\downarrow\rangle,\ |p_x - ip_y,\uparrow\rangle,\ |p_x - ip_y,\downarrow\rangle\}$ in AsO and $\{|d_{xy} + i d_{x^2-y^2},\uparrow\rangle,\ |d_{xy} + i d_{x^2-y^2},\downarrow\rangle,\ |d_{xy} - i d_{x^2-y^2},\uparrow\rangle,\ |d_{xy} - i d_{x^2-y^2},\downarrow\rangle\}$ in $Mo_2TiC_2O_2$, their $k \cdot p$ Hamiltonians can both be written in the form

$$\begin{aligned} H_0(\boldsymbol{k}) &= h_0(\boldsymbol{k})\tau_0 s_0 + \alpha(k_x^2 - k_y^2)\tau_x s_0 + 2\alpha k_x k_y \tau_y s_0 + \lambda \tau_z s_z \\ &= \begin{pmatrix} h_0(\boldsymbol{k})+\lambda & 0 & \alpha k_-^2 & 0 \\ 0 & h_0(\boldsymbol{k})-\lambda & 0 & \alpha k_-^2 \\ \alpha k_+^2 & 0 & h_0(\boldsymbol{k})-\lambda & 0 \\ 0 & \alpha k_+^2 & 0 & h_0(\boldsymbol{k})+\lambda \end{pmatrix}. \end{aligned} \tag{11}$$

Here, $h_0(\boldsymbol{k}) = \varepsilon_0 + c\left(k_x^2 + k_y^2\right), k_\pm = k_x \pm ik_y$, and λ is the SOC strength. τ_i and s_i $(i = 0, x, y, z)$ are Pauli matrices in orbital ($p_x \pm ip_y$ in AsO and $d_{xy} \pm i d_{x^2-y^2}$ in $Mo_2TiC_2O_2$) and spin space. From the calculations using the $k \cdot p$ Hamiltonian, we found that $C_{\uparrow/\downarrow} = \pm 1$, and the spin Chern number is $C_s = \frac{1}{2}(C_\uparrow - C_\downarrow) = 1$. This indicates that the system possesses nontrivial topological properties, consistent with our analysis of the first-principles band structures.

In addition, we also notice that the lowest energy exciton is composed of unlike-spin conduction and valence electrons, arising from the band geometric properties. To see this, we define the effective Coulomb interaction $U_{ij}(\boldsymbol{k}, \boldsymbol{k}') \equiv W(\boldsymbol{k} - \boldsymbol{k}')\Lambda_{ii}(\boldsymbol{k}, \boldsymbol{k}')\Lambda_{jj}(\boldsymbol{k}', \boldsymbol{k})$ as the effective interaction, where $W(\boldsymbol{q}) = 2\pi/\left[|q|\left(1 + 2\pi|q|\alpha_{2D}\right)\right]$ is the screened Coulomb interaction, $i, j \in \{c\uparrow, c\downarrow, v\uparrow, v\downarrow\}$. It is smaller than $W(\boldsymbol{k} - \boldsymbol{k}')$ as a result of the Bloch form factors. As H_0 is isotropic, we can

decompose these quantities into different angular momentum channels, and find[65]

$$U^{1s}_{c\uparrow v\downarrow}(\boldsymbol{k},\boldsymbol{k}') = U^{1s}_{c\downarrow v\uparrow}(\boldsymbol{k},\boldsymbol{k}'), U^{1s}_{c\uparrow v\uparrow}(\boldsymbol{k},\boldsymbol{k}') = U^{1s}_{c\downarrow v\downarrow}(\boldsymbol{k},\boldsymbol{k}'),$$
$$U^{1s}_{c\uparrow v\downarrow}(\boldsymbol{k},\boldsymbol{k}') - U^{1s}_{c\uparrow v\uparrow}(\boldsymbol{k},\boldsymbol{k}') = [W^0(k,k') - W^4(k,k')]\tilde{\Phi}_k\tilde{\Phi}_{k'}, \tag{12}$$

where $W(\boldsymbol{k}_1-\boldsymbol{k}_2) = \sum_m W^m(k_1,k_2)\mathrm{e}^{\mathrm{i}m(\theta_1-\theta_2)}$, $\tilde{\Phi}_k = \Phi_k/4\pi \in (0,1/2)$ and Φ_k is the spin-up valence band's Berry curvature flux through the circle around Γ with radius k. As a result of the long-range nature of the screened Coulomb interaction, $W^0(k,k') > W^4(k,k')$, we can conclude that the effective interaction in a 1s unlike-spin channel is larger than that in a like-spin channel. For trivial bands with zero Berry curvature flux, the like- and unlike-spin 1s excitons are degenerate. Therefore, the spin-triplet nature of the lowest-energy exciton state is closely related to the non-trivial band geometry of H_0.[65,66]

During the formation of the EI phase, the gap remains finite. Therefore, the topology should be identical to the non-interacting case. This can also be verified by the Wilson loop calculations in Ref. [21]. Hartree–Fock calculations[21] further showed that the EI phase persists in a large range of ε_r with the critical value being $\varepsilon_{\mathrm{r},c} = 6.7$ for AsO and $\varepsilon_{\mathrm{r},c} = 9.6$ for $Mo_2TiC_2O_2$, indicating that the EI phase is achievable on realistic substrates in experiments.

In this EI phase, there is no charge density wave as the excitons condense at $Q = 0$, and ferroelectricity does not exist either due to the same parity of the CBM and VBM. To experimentally detect this phase, we can exploit the rotational symmetry breaking, which results from the s-wave excitonic order parameters. The broken rotational symmetry of the electronic system may affect the lattice symmetry through the electron–phonon coupling, which can be probed through experiments such as x-ray diffraction and STM. Additionally, as shown in Fig. 3(b), the absorption spectrum will also be anisotropic, which can be demonstrated by the real part of the optical conductivity

$$\sigma_a(\omega) = \frac{1}{\Omega}\sum_{m\in c,n\in v}\sum_{\boldsymbol{k}}\frac{4\mathrm{i}e^2\omega\mathcal{O}^a_{\boldsymbol{k},nm}\left(f_\mathrm{F}(E_{\boldsymbol{k},n}) - f_\mathrm{F}(E_{\boldsymbol{k},m})\right)}{\hbar\omega + \mathrm{i}0^+ + E_{\boldsymbol{k},n} - E_{\boldsymbol{k},m}}, \tag{13}$$

$$\mathcal{O}^a_{\boldsymbol{k},nm} = \frac{\hbar^2\left|\hat{v}^a_{nm}(\boldsymbol{k})\right|^2}{\left(E_{\boldsymbol{k},n} - E_{\boldsymbol{k},m}\right)^2}. \tag{14}$$

A large number of spin-triplet excitons emerge spontaneously when the topological EI is achieved. For the $c\uparrow v\downarrow$ ($c\downarrow v\uparrow$) exciton, or the e$\uparrow$ h$\uparrow$ (e$\downarrow$ h$\downarrow$) exciton equivalently, the electron and hole have Berry curvature with opposite signs ($\Omega^\uparrow_\mathrm{e}, \Omega^\downarrow_\mathrm{h} < 0$ and $\Omega^\downarrow_\mathrm{e}, \Omega^\uparrow_\mathrm{h} > 0$). From the semiclassical equations of motion for the exciton $\dot{\boldsymbol{K}} = \dot{\boldsymbol{k}}_\mathrm{e} + \dot{\boldsymbol{k}}_\mathrm{h} = 0, \dot{\boldsymbol{R}} = (\partial_{\boldsymbol{k}_\mathrm{e}}\varepsilon^\mathrm{e}_{\boldsymbol{k}_\mathrm{e}} + \partial_{\boldsymbol{k}_\mathrm{h}}\varepsilon^\mathrm{h}_{\boldsymbol{k}_\mathrm{h}})/2 - \dot{\boldsymbol{k}}_\mathrm{e}\times(\boldsymbol{\Omega}_\mathrm{e} - \boldsymbol{\Omega}_\mathrm{h})/2$, we can see that the spin-triplet exciton acquires velocity in the transverse direction.[67] This results in a net transverse spin transport, as shown in Fig. 4(c), which can be identified as an exciton spin-Hall effect. Here the spin Hall conductivity can be calculated using[68,69]

$$\sigma^{s_z}_{xy}(\omega) = \sum_{mn,m\neq n}\sum_{\boldsymbol{k}}\frac{-2\hbar e f_\mathrm{F}(E_{\boldsymbol{k},n})\,\mathrm{Im}\left[\hat{j}^{s_z}_{x,nm}(\boldsymbol{k})\hat{v}^y_{mn}(\boldsymbol{k})\right]}{\left(E_{\boldsymbol{k},n} - E_{\boldsymbol{k},m}\right)^2 - (\hbar\omega + \mathrm{i}0^+)^2}, \tag{15}$$

where $\hat{j}^{s_z}_x$ is the spin current operator. As shown in Fig. 3(d), the spin Hall conductivity is non-zero in the topological EI phase. In summary, the topological properties can be verified through ARPES measurements of edge states, while the transition to the TEI phase can be identified by the anisotropy in optical absorption spectra and the reduction of spin Hall conductivity below unity. All these experimental probes are currently accessible with state-of-the-art techniques.

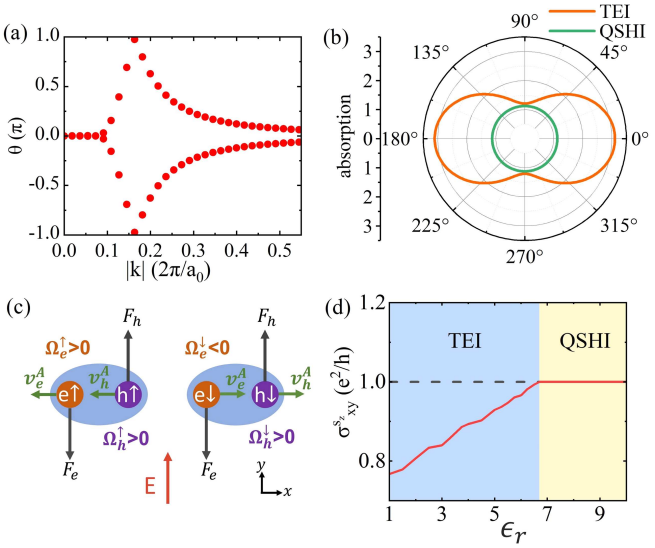


Fig. 3. (a) Results of Wilson-loop calculation for the topological excitonic insulator (TEI) phase, where the red dots represent the phase angles of the two occupied bands. (b) Absorption intensity at $\omega = 0.4$ eV with different polarization directions. (c) A schematic diagram for the exciton spin-Hall effect. The electron and hole for each spin-triplet exciton will obtain an anomalous velocity $\boldsymbol{v}^\mathrm{A}_{\mathrm{e/h}} = -\dot{\boldsymbol{k}}_{\mathrm{e/h}}\times\boldsymbol{\Omega}_{\mathrm{e/h}}$ pointing in the same direction. (d) Static spin Hall conductivity with respect to different ε_rs. (b) and (d) are calculated at 0 K using AsO parameters. This figure is adopted from Ref. [21].

4. Heterostructures

Since excitons are neutral bosonic quasiparticles composed of electrons and holes, in principle, they can undergo BEC and also exhibit superfluidity. To achieve this phase, attention must be directed toward EIs formed in composite quantum well structures, rather than intrinsic EIs. This is because the hybridization between the conduction and valence bands is unavoidable in intrinsic EI materials, which breaks the individual $U(1)$ symmetries of the electrons and holes.[70] In this scenario, the EI phase transition corresponds only to the breaking of discrete symmetry. As a result, the continuous phase

modes in such materials will exhibit a gap, preventing the realization of true exciton superfluidity.[14–16,70] In contrast to this, in composite quantum well structures, the electron and hole layers are separated by large-gap semiconducting materials such as hBN, which significantly reduces tunneling between the electron and hole layers. Thus, their individual $U(1)$ symmetries can remain nearly intact.

Numerous theoretical works have predicted many nontrivial phenomena in p-wave exciton superfluid, including topologically protected vortex zero modes, charge fractionalization, parity anomalies, and non-Abelian braiding,[71–75] while all experimentally realized exciton condensation systems are s-wave like, including graphene and TMD systems.[29,30,32–34,76–79] One feature in common among previous works is that the band edges are described by the effective mass model, which is qualitatively wrong for gapped chiral fermion (GCF) systems where the band geometry matters. Many physical properties, such as linear and nonlinear optical absorption spectra[65,66,80–83] and spin/charge transport properties,[84–87] are related to band geometric effects, which cannot be captured by the effective mass model. Many 2D materials can be described by GCF systems, e.g., gapped graphene monolayers and multilayers,[88] gapped topological surface states,[89] and many TMD monolayers, including MoS_2.[84] Based on these considerations, we performed a detailed exploration of the exciton condensation in GCF systems with band geometry taken into account in Ref. [20].

The 2D isotropic GCF model Hamiltonian for a single valley can be written as[81]

$$H_{\mathrm{GCF}} = \begin{pmatrix} D & \alpha k^{|w|}\, \mathrm{e}^{\mathrm{i}w\theta_{\boldsymbol{k}}} \\ \alpha k^{|w|}\, \mathrm{e}^{-\mathrm{i}w\theta_{\boldsymbol{k}}} & -D \end{pmatrix}. \tag{16}$$

Here, $2D > 0$ is the energy gap at $\boldsymbol{k} = 0$ measured from the valley and $\theta_{\boldsymbol{k}}$ is the polar angle of $\boldsymbol{k}$. $|w| = 1$ and $|w| = 2$ are the most common cases. TMDs and gapped graphene correspond to $|w| = 1$, while gated bilayer graphene[88] and the topological EIs[21] discussed in Subsection 3.3 correspond to $|w| = 2$. The eigenenergies are $\varepsilon_{c/v} = \pm\varepsilon_k = \pm\sqrt{D^2 + \alpha^2 k^{2|w|}}$, with eigenstates

$$|c\boldsymbol{k}\rangle = \begin{pmatrix} \cos\frac{\phi_k}{2} \\ \sin\frac{\phi_k}{2}\, \mathrm{e}^{-\mathrm{i}w\theta_{\boldsymbol{k}}} \end{pmatrix}, \quad |v\boldsymbol{k}\rangle = \begin{pmatrix} \sin\frac{\phi_k}{2}\, \mathrm{e}^{\mathrm{i}w\theta_{\boldsymbol{k}}} \\ -\cos\frac{\phi_k}{2} \end{pmatrix}, \tag{17}$$

where $\phi_k = \arccos(D/\varepsilon_k), \phi_k \in (0, \pi/2)$. Using this gauge, the lowest energy exciton state is a 1s state in the 2D hydrogen model.[65,81]

The double-layer exciton condensation heterostructure is demonstrated in Fig. 4(a). Each layer is described by a GCF model, with the top (bottom) layer separately gated by V_{t} (V_{b}), ensuring that the top (bottom) layer has electron (hole) Fermi surfaces. Charge neutrality is assumed ($V_{\mathrm{g,t}} = -V_{\mathrm{g,b}} = -V_{\mathrm{g}}$), and the electron and hole Fermi surfaces are perfectly nested as shown in Fig. 4(b), favoring the excitonic instability the most. By taking the electron–hole interaction into consideration, the formation of inter-layer exciton condensation will open a gap (Fig. 4(c)), and the system will evolve from a semimetal to an EI state.

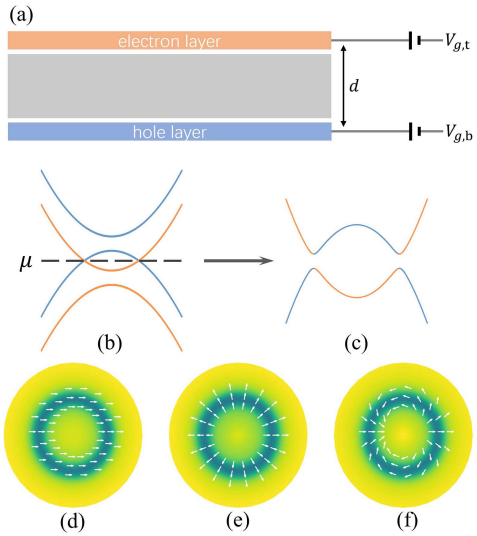


Fig. 4. (a) Schematic for the exciton condensation heterostructure. The electron and hole layers are separated in the z direction with width d. (b) At the charge neutrality point, the electron and hole Fermi surfaces are perfectly nested. (c) Excitonic instability is favored, and a gap opens. Here the orange (blue) lines indicate the bands from the top (bottom) layer. (d)–(f) s-, p-, d-wave like excitonic order parameters. The direction of the arrow denotes the phase angle and the darkness of the colormap indicates the magnitude.

The non-interacting Hamiltonian for the two-layer system in the two-band basis reads

$$H_0 = \sum_{\boldsymbol{k}} \Psi_{\boldsymbol{k}}^{\dagger} \begin{pmatrix} V_{\mathrm{g,t}} + \varepsilon_{c\boldsymbol{k},\mathrm{t}} & 0 \\ 0 & V_{\mathrm{g,b}} + \varepsilon_{v\boldsymbol{k},\mathrm{b}} \end{pmatrix} \Psi_{\boldsymbol{k}}, \tag{18}$$

where $\Psi_{\boldsymbol{k}}^{\dagger} = \left[c_{c\boldsymbol{k},\mathrm{t}}^{\dagger}, c_{v\boldsymbol{k},\mathrm{b}}^{\dagger}\right]$. Here, $c_{c\boldsymbol{k},\mathrm{t}}$ ($c_{v\boldsymbol{k},\mathrm{b}}$) refers to the electrons in the conduction (valence) band of the top (bottom) layer in Fig. 4(b). The interlayer interaction between these two bands reads

$$\begin{aligned} H_{\mathrm{int}} = & \sum_{\boldsymbol{k}_1,\boldsymbol{k}_2,\boldsymbol{q}} V_{\mathrm{inter}}(q) \Lambda_{cc}(\boldsymbol{k}_1, \boldsymbol{k}_1 - \boldsymbol{q}) \Lambda_{vv}(\boldsymbol{k}_2, \boldsymbol{k}_2 + \boldsymbol{q}) \\ & \times c_{c\boldsymbol{k}_1,\mathrm{t}}^{\dagger} c_{v\boldsymbol{k}_2,\mathrm{b}}^{\dagger} c_{v\boldsymbol{k}_2+\boldsymbol{q},\mathrm{b}} c_{c\boldsymbol{k}_1-\boldsymbol{q},\mathrm{t}}, \end{aligned} \tag{19}$$

where $V_{\mathrm{inter}}(q)$ is the interlayer screened Coulomb interaction, $\Lambda_{ab}(\boldsymbol{k}, \boldsymbol{p}) \equiv \langle a\boldsymbol{k} \mid b\boldsymbol{p}\rangle$ is the form factor where $a, b \in \{c, v\}$. In the GCF model, it deviates from unity:

$$\begin{aligned} \Lambda_{cc}(\boldsymbol{k}, \boldsymbol{p}) = & \cos\left(\frac{\phi_{ck}}{2}\right) \cos\left(\frac{\phi_{cp}}{2}\right) \\ & + \sin\left(\frac{\phi_{ck}}{2}\right) \sin\left(\frac{\phi_{cp}}{2}\right) \mathrm{e}^{\mathrm{i}m(\theta_{\boldsymbol{k}} - \theta_{\boldsymbol{p}})}, \\ \Lambda_{vv}(\boldsymbol{k}, \boldsymbol{p}) = & \cos\left(\frac{\phi_{vk}}{2}\right) \cos\left(\frac{\phi_{vp}}{2}\right) \\ & + \sin\left(\frac{\phi_{vk}}{2}\right) \sin\left(\frac{\phi_{vp}}{2}\right) \mathrm{e}^{-\mathrm{i}n(\theta_{\boldsymbol{k}} - \theta_{\boldsymbol{p}})}, \end{aligned} \tag{20}$$

where m (n) is the chiral winding number for the conduction (valence) band.

The correlation between the angular momentum of the exciton condensation and the band geometry becomes clearer when we project the interaction onto the Fermi surfaces, which is valid in the BCS regime as the pairing order parameter is mainly localized around the narrow regions of the Fermi surfaces.[37,90–96] Therefore, we can use the Fermi surface projected interlayer interaction, defined as $U_{m,n}(k_{\rm F},\theta_1,\theta_2) \equiv V_{\rm inter}(k_{\rm F},\theta_1,\theta_2)\Lambda_{cc}(k_{\rm F},\theta_1,\theta_2)\Lambda_{vv}(k_{\rm F},\theta_2,\theta_1)$, to perform an analysis of the angular dependence of the pairing. Decomposing $U_{m,n}$, $V_{\rm inter}$, Λ_{cc}, and Λ_{vv} into different angular momentum channels and using the convolution rules, we obtain the interaction in each channel J:

$$U^J_{m,n}(k_{\rm F}) = \sum_{J_1+J_2-J_3=J} V^{J_1}_{\rm inter}(k_{\rm F})\Lambda^{J_2}_{cc}(k_{\rm F})\Lambda^{J_3}_{vv}(k_{\rm F}). \quad (21)$$

The excitonic pairing is characterized by the channel with the largest $U^J_{\rm inter}(k_{\rm F})$.

As detailed in Ref. [20], Λ^Js satisfy the following relations in general rotationally symmetric models, as $\sum_J \Lambda^J = 1$, $\sum_J J\Lambda^J = \frac{\Phi}{2\pi}$, where Φ is the Berry curvature flux through the Fermi surfaces. In the GCF model, only Λ^0_{cc}, Λ^0_{vv}, Λ^m_{cc} and Λ^{-n}_{vv} are non-zero according to Eq. (20), and the above relations reduce to $\Lambda^0_{cc} = 1-\tilde{\Phi}_c/m$, $\Lambda^0_{vv} = 1-\tilde{\Phi}_v/n$, $\Lambda^m_{cc} = \tilde{\Phi}_c/m$, $\Lambda^{-n}_{vv} = \tilde{\Phi}_v/n$, where $\tilde{\Phi} = \Phi/2\pi \in (-|m|/2, |m|/2)$. Taking the long-range form of the $V_{\rm inter}$ into consideration, the s-to-p transition line is obtained for $m = n = 1$ in Fig. 5(a) (dashed green line), which closely matches the full numerical calculations (solid green line). The excitonic condensation exhibits s-wave (p-wave)-like behavior when the Berry curvature flux is small (large), which is discussed in detail in Ref. [20]. It is important to note that in the trivial case where the form factor is unity, excitonic pairing always occurs in the $J = 0$ channel, as $V^{J=0}_{\rm inter}$ is always the largest for realistic long-range Coulomb interactions. Thus, the GCF model clearly demonstrates the essential role of band geometry effects in the high-angular momentum excitonic condensation.

Based on the above analysis, we propose that staggered graphene and magnetic topological surface states are promising candidate material systems to realize p-wave exciton condensation.[20] The change in anomalous Hall conductivity can serve as experimental evidence for the p-wave exciton condensation,[97] as shown in Fig. 5(b). Without interactions, the Chern numbers of the two valence bands are both $-1/2$ since the chiral winding numbers are both $+1$ in the top and bottom layers. Consequently, the overall anomalous Hall conductivity for this semimetallic system is

$$\sigma_{\rm AHC} = \frac{e^2}{\hbar}\int_{\rm occupied}\frac{{\rm d}^2k}{(2\pi)^2}\Omega_{n,\boldsymbol{k}} = \left(\tilde{\Phi}_{c,{\rm t}} - \tilde{\Phi}_{v,{\rm b}} - 1\right)\frac{e^2}{h}.$$

When the electron–hole interaction is included, the system is driven into the insulating EI phase. The Chern numbers of the valence bands remain $-1/2, -1/2$ if the pairing is s-wave, and become $1/2, -1/2$ if the pairing is p-wave. The anomalous Hall conductivity of the system becomes $\sigma^{\rm s}_{\rm AHC} = [(-\frac{1}{2})+(-\frac{1}{2})]\frac{e^2}{h} = -\frac{e^2}{h}$ for the s-wave pairing and $\sigma^{\rm p}_{\rm AHC} = [(\frac{1}{2})+(-\frac{1}{2})]\frac{e^2}{h} = 0$ for the p-wave pairing.

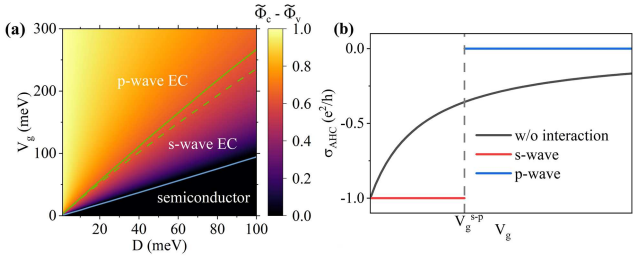


Fig. 5. (a) The phase diagram when the electron and hole layers are both $m = 1$ GCF model, and $\alpha = 10^6$ m/s. The dielectric constant of the heterostructure is $\varepsilon_{\rm r} = 5$, and the distance between the two layers is $d = 4$ nm. The solid lines are obtained by self-consistent calculations, and the dashed line is determined by the Fermi surface projection. The colorbar indicates the Berry curvature flux. EC means exciton condensation. (b) Anomalous Hall conductivity with (red and blue lines) and without (black solid line) electron–hole interactions in the setup are shown in the inset when the gating is increased. This figure is adopted from Ref. [20].

5. Conclusions and outlook

In this paper, we review some new progress in the search for EIs in two-dimensional systems from theoretical and computational perspectives, with results published in Refs. [19–21] taken as the basis. Two general strategies to find EIs in intrinsic materials are discussed, using EIs in small indirect-gap 2D materials and EIs in QSHIs with a particular type of band inversion as examples. A novel approach to achieving high-angular momentum EIs in heterostructures is also given, with analysis on the influence of the band geometry provided. Meanwhile, experimental signatures for detecting EIs in each case are discussed. Although the necessary experimental techniques are readily available, our predictions have yet to be experimentally validated. This presents a valuable opportunity for experimentalists to investigate these novel quantum phenomena.

Several future directions in EI physics are worth exploring. First, since screening effects are further reduced in one-dimensional (1D) systems, EIs in such systems deserve more detailed investigation. Recent studies have indeed demonstrated the existence of EIs in various 1D systems.[98–100] Second, intrinsic materials should be studied more thoroughly in the context of EIs. The symmetry breaking in intrinsic EIs is not continuous. This precludes the possibility of superfluidity in them. However, other interesting properties remain unexplored and warrant further investigation. For example, theoretical descriptions of the exciton Nernst effect and the thermal Hall effect call for attention. The effects of exciton–phonon coupling, exciton–exciton interactions, and exchange interactions also deserve further exploration. Recently, a novel CDW-like finite-momentum EI was predicted

in WSe_2 monolayer.[101] Third, experimental signatures and the potential anomalous properties of exciton superfluidity in heterostructures also call for further studies. For example, it would be intriguing to explore whether exciton backflow superfluidity could be utilized in the design of novel Josephson junction devices. Considering the fundamental importance of quantum phases beyond the band theory in condensed matter physics, further theoretical and experimental studies on this topic are highly desirable.

Acknowledgements

X.-Z. Li is supported by the National Key Research & Development Program of China (Grant Nos. 2022YFA1403500 and 2021YFA1400500) and the National Science Foundation of China (Grant Nos. 62321004, 12234001, and 12474215). The computational resources are provided by the supercomputer center at Peking University, China. X. Dai is supported by New Cornerstone Science Foundation and a fellowship and a CRF award from the Research Grants Council of the Hong Kong Special Administrative Region, China (Grant Nos. HKUST SRFS2324-6S01 and C7037-22GF).

References

[1] Frenkel J 1931 *Phys. Rev.* **37** 17
[2] Wannier G H 1937 *Phys. Rev.* **52** 191
[3] Rohlfing M and Louie S G 2000 *Phys. Rev. B* **62** 4927
[4] Chernikov A, Berkelbach T C, Hill H M, Rigosi A, Li Y, Aslan B, Reichman D R, Hybertsen M S and Heinz T F 2014 *Phys. Rev. Lett.* **113** 076802
[5] Ugeda M M, Bradley A J, Shi S F, Da Jornada F H, Zhang Y, Qiu D Y, Ruan W, Mo S K, Hussain Z, Shen Z X, *et al*. 2014 *Nat. Mater.* **13** 1091
[6] Bhimanapati G R, Lin Z, Meunier V, Jung Y, Cha J, Das S, Xiao D, Son Y, Strano M S, Cooper V R, *et al*. 2015 *ACS Nano* **9** 11509
[7] Novoselov K S, Mishchenko A, Carvalho A and Castro Neto A 2016 *Science* **353** aac9439
[8] Kovalenko M V, Protesescu L and Bodnarchuk M I 2017 *Science* **358** 745
[9] Girvin S M and Yang K 2019 *Modern Condensed Matter Physics* (Cambridge University Press)
[10] Keldysh L and Kopaev Y V 1965 *Soviet Physics Solid State, USSR* **6** 2219
[11] Kohn W 1967 *Phys. Rev. Lett.* **19** 439
[12] Jérome D, Rice T and Kohn W 1967 *Phys. Rev.* **158** 462
[13] Halperin B and Rice T 1968 *Rev. Mod. Phys.* **40** 755
[14] Murakami Y, Golež D, Kaneko T, Koga A, Millis A J and Werner P 2020 *Phys. Rev. B* **101** 195118
[15] Golež D, Sun Z, Murakami Y, Georges A and Millis A J 2020 *Phys. Rev. Lett.* **125** 257601
[16] Sun Z, Kaneko T, Golež D and Millis A J 2021 *Phys. Rev. Lett.* **127** 127702
[17] Kaneko T, Sun Z, Murakami Y, Golež D and Millis A J 2021 *Phys. Rev. Lett.* **127** 127402
[18] Shao Y and Dai X 2024 *Phys. Rev. X* **14** 021047
[19] Yang H, Wang X and Li X Z 2022 *New J. Phys.* **24** 083010
[20] Yang H, Shao Y, Xu Y, Dai X and Li X Z 2024 *Phys. Rev. B* **109** L201401
[21] Yang H, Zeng J, Shao Y, Xu Y, Dai X and Li X Z 2024 *Phys. Rev. B* **109** 075167
[22] Du L, Li X, Lou W, Sullivan G, Chang K, Kono J and Du R R 2017 *Nat. Commun.* **8** 1
[23] Wang R, Sedrakyan T A, Wang B, Du L and Du R R 2023 *Nature* **619** 57
[24] Mazza G, Rösner M, Windgätter L, Latini S, Hübener H, Millis A J, Rubio A and Georges A 2020 *Phys. Rev. Lett.* **124** 197601
[25] Jiang Z, Li Y, Zhang S and Duan W 2018 *Phys. Rev. B* **98** 081408
[26] Jiang Z, Li Y, Duan W and Zhang S 2019 *Phys. Rev. Lett.* **122** 236402
[27] Jiang Z, Lou W, Liu Y, Li Y, Song H, Chang K, Duan W and Zhang S 2020 *Phys. Rev. Lett.* **124** 166401
[28] Sethi G, Zhou Y, Zhu L, Yang L and Liu F 2021 *Phys. Rev. Lett.* **126** 196403
[29] Wang Z, Rhodes D A, Watanabe K, Taniguchi T, Hone J C, Shan J and Mak K F 2019 *Nature* **574** 76
[30] Ma L, Nguyen P X, Wang Z, Zeng Y, Watanabe K, Taniguchi T, MacDonald A H, Mak K F and Shan J 2021 *Nature* **598** 585
[31] Liu X, Li J, Watanabe K, Taniguchi T, Hone J, Halperin B I, Kim P and Dean C R 2022 *Science* **375** 205
[32] Jia Y, Wang P, Chiu C L, Song Z, Yu G, Jäck B, Lei S, Klemenz S, Cevallos F A, Onyszczak M, *et al*. 2022 *Nat. Phys.* **18** 87
[33] Sun B, Zhao W, Palomaki T, Fei Z, Runburg E, Malinowski P, Huang X, Cenker J, Cui Y T, Chu J H, *et al*. 2022 *Nat. Phys.* **18** 94
[34] Gu J, Ma L, Liu S, Watanabe K, Taniguchi T, Hone J C, Shan J and Mak K F 2022 *Nat. Phys.* **18** 395
[35] Bardeen J, Cooper L N and Schrieffer J R 1957 *Phys. Rev.* **106** 162
[36] Kozlov A N and Maksimov L A 1966 *Sov. Phys. JETP* **23** 88
[37] Littlewood P, Eastham P, Keeling J, Marchetti F, Simons B and Szymanska M 2004 *J. Phys.: Condens. Matter* **16** S3597
[38] Bronold F X and Fehske H 2006 *Phys. Rev. B* **74** 165107
[39] Phan V N, Becker K W and Fehske H 2010 *Phys. Rev. B* **81** 205117
[40] Seki K, Eder R and Ohta Y 2011 *Phys. Rev. B* **84** 245106
[41] Perfetto E, Sangalli D, Marini A and Stefanucci G 2019 *Phys. Rev. Materials* **3** 124601
[42] Cercellier H, Monney C, Clerc F, Battaglia C, Despont L, Garnier M G, Beck H, Aebi P, Patthey L, Berger H and Forró L 2007 *Phys. Rev. Lett.* **99** 146403
[43] Kogar A, Rak M S, Vig S, Husain A A, Flicker F, Joe Y I, Venema L, MacDougall G J, Chiang T C, Fradkin E, *et al*. 2017 *Science* **358** 1314
[44] Wakisaka Y, Sudayama T, Takubo K, Mizokawa T, Arita M, Namatame H, Taniguchi M, Katayama N, Nohara M and Takagi H 2009 *Phys. Rev. Lett.* **103** 026402
[45] Lu Y, Kono H, Larkin T, Rost A, Takayama T, Boris A, Keimer B and Takagi H 2017 *Nat. Commun.* **8** 14408
[46] Mor S, Herzog M, Golez D, Werner P, Eckstein M, Katayama N, Nohara M, Takagi H, Mizokawa T, Monney C and Stahler J 2017 *Phys. Rev. Lett.* **119** 086401
[47] Choi J H, Cui P, Lan H and Zhang Z 2015 *Phys. Rev. Lett.* **115** 066403
[48] Jiang Z, Liu Z, Li Y and Duan W 2017 *Phys. Rev. Lett.* **118** 266401
[49] Rasmussen F A and Thygesen K S 2015 *The Journal of Physical Chemistry C* **119** 13169
[50] Thygesen K S 2017 *2D Mater.* **4** 022004
[51] Fiori G, Bonaccorso F, Iannaccone G, Palacios T, Neumaier D, Seabaugh A, Banerjee S K and Colombo L 2014 *Nat. Nanotechnol.* **9** 768
[52] Gao Q, Chan Yh, Jiao P, Chen H, Yin S, Tangprapha K, Yang Y, Li X, Liu Z, Shen D, *et al*. 2024 *Nat. Phys.* **20** 597
[53] Kane C L and Mele E J 2005 *Phys. Rev. Lett.* **95** 226801
[54] Kane C L and Mele E J 2005 *Phys. Rev. Lett.* **95** 146802
[55] Liu C, Hughes T L, Qi X L, Wang K and Zhang S C 2008 *Phys. Rev. Lett.* **100** 236601
[56] Bernevig B A, Hughes T L and Zhang S C 2006 *Science* **314** 1757
[57] Kou L, Ma Y, Sun Z, Heine T and Chen C 2017 *The Journal of Physical Chemistry Lett.* **8** 1905
[58] Lodge M S, Yang S A, Mukherjee S and Weber B 2021 *Advanced Materials* **33** 2008029
[59] Fu L and Kane C L 2007 *Phys. Rev. B* **76** 045302
[60] Dong S and Li Y 2023 *Phys. Rev. B* **107** 235147
[61] Si C, Jin K H, Zhou J, Sun Z and Liu F 2016 *Nano Lett.* **16** 6584
[62] Wang Y, Ji W, Zhang C, Li P, Zhang S, Wang P, Li S and Yan S 2017 *Appl. Phys. Lett.* **110** 213101
[63] Xu Y, Yan B, Zhang H J, Wang J, Xu G, Tang P, Duan W and Zhang S C 2013 *Phys. Rev. Lett.* **111** 136804
[64] Deng J, Shao D, Gao J, Yue C, Weng H, Fang Z and Wang Z 2022 *Phys. Rev. B* **105** 224103
[65] Zhou J, Shan W Y, Yao W and Xiao D 2015 *Phys. Rev. Lett.* **115** 166803
[66] Srivastava A and Imamoğlu A 2015 *Phys. Rev. Lett.* **115** 166802

[67] Chaudhary S, Knapp C and Refael G 2021 *Phys. Rev. B* **103** 165119
[68] Sinova J, Valenzuela S O, Wunderlich J, Back C H and Jungwirth T 2015 *Rev. Mod. Phys.* **87** 1213
[69] Yao Y and Fang Z 2005 *Phys. Rev. Lett.* **95** 156601
[70] Mazza G, Rosner M, Windgatter L, Latini S, Hubener H, Millis A J, Rubio A and Georges A 2020 *Phys. Rev. Lett.* **124** 197601
[71] Seradjeh B, Weber H and Franz M 2008 *Phys. Rev. Lett.* **101** 246404
[72] Seradjeh B, Moore J E and Franz M 2009 *Phys. Rev. Lett.* **103** 066402
[73] Wang R, Erten O, Wang B and Xing D 2019 *Nat. Commun.* **10** 210
[74] Wu Y, Jiang H, Chen H, Liu H, Liu J and Xie X C 2022 *Phys. Rev. Lett.* **128** 106804
[75] Perfetto E and Stefanucci G 2020 *Phys. Rev. Lett.* **125** 106401
[76] Ponomarenko L, Geim A, Zhukov A, Jalil R, Morozov S, Novoselov K, Grigorieva I, Hill E, Cheianov V, Fal'ko V, *et al*. 2011 *Nat. Phys.* **7** 958
[77] Liu X, Watanabe K, Taniguchi T, Halperin B I and Kim P 2017 *Nat. Phys.* **13** 746
[78] Li J, Taniguchi T, Watanabe K, Hone J and Dean C 2017 *Nat. Phys.* **13** 751
[79] Chen D, Lian Z, Huang X, Su Y, Rashetnia M, Ma L, Yan L, Blei M, Xiang L, Taniguchi T, *et al*. 2022 *Nat. Phys.* **18** 1171
[80] Cao T, Wu M and Louie S G 2018 *Phys. Rev. Lett.* **120** 087402
[81] Zhang X, Shan W Y and Xiao D 2018 *Phys. Rev. Lett.* **120** 077401
[82] Glazov M M, Golub L E, Wang G, Marie X, Amand T and Urbaszek B 2017 *Phys. Rev. B* **95** 035311
[83] Tabert C J and Nicol E J 2013 *Phys. Rev. Lett.* **110** 197402
[84] Xiao D, Liu G B, Feng W, Xu X and Yao W 2012 *Phys. Rev. Lett.* **108** 196802
[85] Lu H Z, Yao W, Xiao D and Shen S Q 2013 *Phys. Rev. Lett.* **110** 016806
[86] Gao Y, Yang S A and Niu Q 2014 *Phys. Rev. Lett.* **112** 166601
[87] Yu H, Wu Y, Liu G B, Xu X and Yao W 2014 *Phys. Rev. Lett.* **113** 156603
[88] McCann E and Fal'ko V I 2006 *Phys. Rev. Lett.* **96** 086805
[89] Garate I and Franz M 2011 *Phys. Rev. B* **84** 045403
[90] Zhu X, Littlewood P B, Hybertsen M S and Rice T M 1995 *Phys. Rev. Lett.* **74** 1633
[91] Bronold F X and Fehske H 2006 *Phys. Rev. B* **74** 165107
[92] Min H, Bistritzer R, Su J J and MacDonald A H 2008 *Phys. Rev. B* **78** 121401
[93] Shim Y P and MacDonald A H 2009 *Phys. Rev. B* **79** 235329
[94] Zhang J and Rossi E 2013 *Phys. Rev. Lett.* **111** 086804
[95] Perali A, Neilson D and Hamilton A R 2013 *Phys. Rev. Lett.* **110** 146803
[96] Conti S, Perali A, Peeters F M and Neilson D 2017 *Phys. Rev. Lett.* **119** 257002
[97] Nagaosa N, Sinova J, Onoda S, MacDonald A H and Ong N P 2010 *Rev. Mod. Phys.* **82** 1539
[98] Zhao Y, Qu H, Zhao J, Kang L and Zhou S 2025 *Nano Lett.* **25** 1108
[99] Liu J, Qu H and Li Y 2024 *New J. Phys.* **26** 103034
[100] Liu J and Li Y 2022 *Phys. Rev. B* **106** 035135
[101] Dong S, Chen Y, Qu H, Lou W K and Chang K 2025 *Phys. Rev. Lett.* **134** 066602